2024 IEEE International Conference on Robotics and Automation (ICRA 2024)
May 13-17, 2024. Yokohama, Japan

Design, Modeling and Analysis of a Spherical Parallel Continuum Manipulator for Nursing Robots

Zhenhua Gong , Chuanxin Ning , Jiejunyi Liang and Ting Zhang*, *Member, IEEE*

***Abstract*—In the healthcare industry, nursing robots have made great contributions, assisting in the delivery of food and medicine as well as the movement and transfer of patients. However, the traditional continuum manipulator often has the problems of limited workspace and weak carrying capacity. Compared with traditional manipulator, the continuum manipulator has the advantages of a small moment of inertia and high dexterity. This paper proposes a original cable-driven parallel continuum manipulator with a spherical parallel mechanism as the continuous segments. Due to the spherical parallel mechanisms' characteristics, the proposed cable-driven spherical parallel continuum manipulator offers many inherent advantages for nursing robots. The prototype is tested and analyzed, and the kinematics and statics are verified. The results show that the cable-driven spherical parallel continuum manipulator for nursing robots has low requirements for workspace, suitable for complex spaces and can have a large carrying capacity.**

***Index Terms*—Continuum manipulator, Cable-driven Continuum Manipulator, Spherical Parallel Continuum Manipulator, Nursing robots.**

I. INTRODUCTION

In the past three years, with the outbreak of the COVID-19 pandemic, most people with inconveniences cannot receive care without the time and space and personnel constraints. The invention of nursing robots has brought great convenience to such people. Nursing robots can assist in the delivery of food and medicine as well as the movement and transfer of patients [1]. Currently, the service industry, military industry, agriculture and other related industries have widely used traditional robotic arms. However, the existing rigid robots are mainly based on mechanical arms with no more than six degrees of freedom, and these robots are not adapted to work in scenarios with limited space or complex layouts with obstacles [2]-[4]. Therefore, the development of redundant robotic structures capable of working in complex shape spaces is now urgently needed. For solving this problem, continuum manipulators are an important method at present[5]. The continuum manipulator with multiple degrees of freedom and flexibility makes it suitable for complex environments with interferences.

In nature, vertebrates such as fish and snakes move mainly rely on the sequential deformation of the vertebral joints. Mollusks like jellyfish and leeches can rely on their skeletal muscles or muscles to achieve continuous deformation [6]. Similar to the structure of animals in nature, the existing continuum manipulators can also be divided into two categories: one is a super-redundant robot with a spine structure [7]-[9], and the other is a spineless continuum manipulator structure [10]-[14]. A hype-redundant robot with a vertebral structure uses a rigid structure as its basic drive unit for higher carrying capacity, but its flexibility is relatively poor. For the continuum manipulator with an invertebrate structure, although the flexibility is increased, the load capacity is also reduced on account of the use of flexible components.

Different from traditional continuum manipulators, A continuum manipulator driven by cables is a new type of manipulator [15]-[17]. Currently, cable-driven continuum manipulators are progressively finding applications across various domains [19]-[21]. Nevertheless, their utilization primarily centers on nursing robots owing to their inherent limitations in stiffness and load capacity. In practical operations, the manipulators' motion precision is compromised due to factors like the manipulator's weight and load, resulting in reduced carrying capacity of the robotic arm. During the exercise of rope-driven continuous manipulators [22]-[24], due to factors such as the structure of the continuum, the bending characteristics of the elastic body, and the driving method, the continuous manipulator has disadvantages, for example, the poor ability to resist external force and elastic deformation.

Parallel mechanisms have several unique properties compared with series mechanisms, including greater stiffness, enhanced load capacity, and greater precision. The movable platform of the spherical mechanisms rotates around a physical center or a virtual center [25]-[26]. As a result, a spherical mechanism-based continuum manipulator can obtain a larger workspace, greater stiffness, higher load capacity, and greater precision. In this paper, a original cable-driven spherical parallel continuum robot composed of continuous segments with spherical parallel joints is introduced. Due to the spherical parallel mechanisms, the proposed cable-driven spherical parallel continuum manipulator offers many inherent advantages for nursing robots. The kinematics and statistics are verified by

This work was supported in part by the National Key R&D Program of China (2020YFC2007804), Jiangsu Frontier Leading Technology Fundamental Research Project (BK20192004D), Natural Science Foundation of the Jiangsu Higher Education Institutions of China (19KJA180009), Natural Science Foundation of Jiangsu Province (BK20191424). (Corresponding author: Ting Zhang)

Z. Gong, C. Ning, T. Zhang are with the Robotics and Microsystems Center, College of Mechanical and Electrical Engineering, Soochow University, Suzhou 215000, China. (e-mail: zhangt.hit@gmail. com).
J. Lang is with the School of Mechanical Science and Engineering, Huazhong University of Science and Technology, Wuhan 430074, China

experiments, contributing to the further deepening of the continuum manipulators.

II. DESIGN OF CABLE-DRIVEN SPHERICAL PARALLEL CONTINUUM MANIPULATOR

The proposed spherical parallel continuum manipulator is composed of multiple serially connected spherical parallel mechanisms in Fig. 1(a). The Parallel mechanism joins in sequence by rigid links to constitute the continuous manipulator in this design, it's mainly composed of a series of linkage mechanisms, a static platform, and a movable platform. The movable platform is connected to the fixed platform placed at the bottom of the platform through three evenly distributed linkage mechanisms. The driven link mechanism includes a driving link and a driven link. The driving link and driven link are connected in series, both ends of the active link are connected to the driven link and the static platform in turn through a rotating pair, and a spherical pair is used to connect the driven link and the movable platform of the parallel mechanism. The three-dimensional graph of the structure is shown in Fig. 1(b).

Each spherical parallel mechanism in mechanism controls its movement through three ropes. The rope drives each part of the spherical parallel mechanism to rotate through the cam, thereby driving the movement of the entire parallel manipulator. The spherical parallel mechanism of each

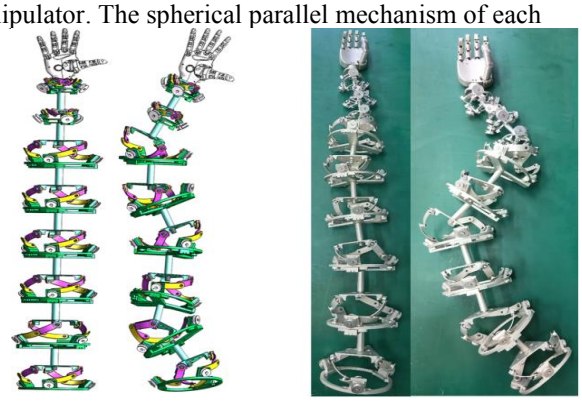

(a) CAD model and prototype of the cable-driven spherical parallel continuum manipulator

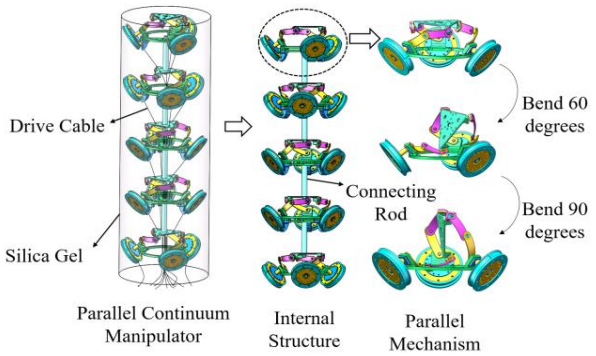

(b) Parallel continuum manipulator structure

Fig. 1. Cable-driven spherical parallel continuum manipulator.

section can also be independently driven and controlled independently. The spherical parallel mechanism designed in this paper can realize three degrees of freedom motion through rope transmission, and the continuum manipulator formed by the multi-section spherical parallel mechanism in series can meet different workspace requirements.

III. THE KINEMATICS OF CONTINUUM MANIPULATOR

A. The Kinematics of parallel mechanism

The kinematic theoretical model of the spherical parallel mechanism proposed is shown in Fig. 2. This is connected by a mobile platform, a static platform and a linkage mechanism in turn. The linkage mechanism consists of three identical structures, each consisting of a driving part and an executing part.

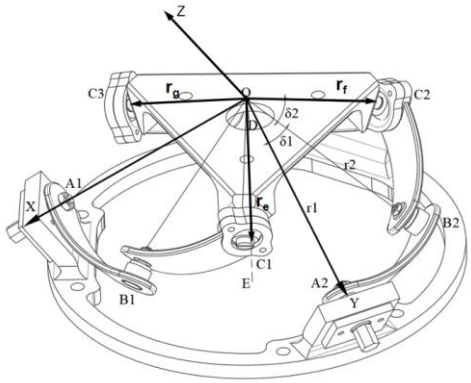

Fig. 2. The kinematic theoretical model of the spherical parallel mechanism

Each link mechanism has two revolute R and one ball pair. Point O is set at the intersection point of the three rotating auxiliary axes on the fixed platform. A_i, B_i and $C_i (i = 1, 2, 3)$ are all located on the centerline of the joint motion pair in turn. Establish the movable coordinate system $\boldsymbol{O-xyz}$ on the movable platform, and $\boldsymbol{O-x}$,$\boldsymbol{O-y}$ and $\boldsymbol{O-z}$ pass through points $\boldsymbol{C_1}$, $\boldsymbol{C_2}$ and $\boldsymbol{C_3}$ on the movable platform respectively. Establish the fixed Coordinate System $\boldsymbol{O-XYZ}$ is established on the bottom member of the parallel mechanism and rays $\boldsymbol{O-X}$, $\boldsymbol{O-Y}$ and $\boldsymbol{O-Z}$ pass through points $\boldsymbol{A_1}$, $\boldsymbol{A_2}$ and $\boldsymbol{A_3}$ respectively. For branch chain 1 of the spherical six-bar chain-leg, the movable screw system is given as

$$\boldsymbol{S_{b1}} = \begin{cases} \boldsymbol{S_{e1}} = (\boldsymbol{s_{e1}}\ \boldsymbol{0}) \\ \boldsymbol{S_{e2}} = (\boldsymbol{s_{e2}}\ \boldsymbol{0}) \\ \boldsymbol{S_{e3}} = (\boldsymbol{s_{e3}}\ \ \boldsymbol{r_e} \times \boldsymbol{s_{e3}}) \\ \boldsymbol{S_{e4}} = (\boldsymbol{s_{e4}}\ \ \boldsymbol{r_e} \times \boldsymbol{s_{e4}}) \\ \boldsymbol{S_{e5}} = (\boldsymbol{s_{e5}}\ \ \boldsymbol{r_e} \times \boldsymbol{s_{e5}}) \end{cases} \tag{1}$$

For branch chain 2,the movable screw system is given by

$$\boldsymbol{S_{b2}} = \begin{cases} \boldsymbol{S_{f1}} = (\boldsymbol{s_{f1}}\ \boldsymbol{0}) \\ \boldsymbol{S_{f2}} = (\boldsymbol{s_{f2}}\ \boldsymbol{0}) \\ \boldsymbol{S_{f3}} = (\boldsymbol{s_{f3}}\ \ \boldsymbol{r_f} \times \boldsymbol{s_{f3}}) \\ \boldsymbol{S_{f4}} = (\boldsymbol{s_{f4}}\ \ \boldsymbol{r_f} \times \boldsymbol{s_{f4}}) \\ \boldsymbol{S_{f5}} = (\boldsymbol{s_{f5}}\ \ \boldsymbol{r_f} \times \boldsymbol{s_{f5}}) \end{cases} \tag{2}$$

For branch chain 3,the movable screw system is given by

$$\boldsymbol{S_{b3}} = \begin{cases} \boldsymbol{S_{g1}} = (\boldsymbol{s_{g1}}\ \boldsymbol{0}) \\ \boldsymbol{S_{g2}} = (\boldsymbol{s_{g2}}\ \boldsymbol{0}) \\ \boldsymbol{S_{g3}} = (\boldsymbol{s_{g3}}\ \ \boldsymbol{r_g} \times \boldsymbol{s_{g3}}) \\ \boldsymbol{S_{g4}} = (\boldsymbol{s_{g4}}\ \ \boldsymbol{r_g} \times \boldsymbol{s_{g4}}) \\ \boldsymbol{S_{g5}} = (\boldsymbol{s_{g5}}\ \ \boldsymbol{r_g} \times \boldsymbol{s_{g5}}) \end{cases} \tag{3}$$

Where $\boldsymbol{s_{e1}} = \boldsymbol{s_{e3}}, \boldsymbol{s_{f1}} = \boldsymbol{s_{f3}}, \boldsymbol{s_{g1}} = \boldsymbol{s_{g3}}$.

The constrained reciprocal screw system corresponding to each branch is easily derived.

$$\boldsymbol{S_b^r} = \begin{cases} \boldsymbol{S_{b1}^r} = (\boldsymbol{r_e}\ \boldsymbol{0}) \\ \boldsymbol{S_{b2}^r} = (\boldsymbol{r_f}\ \boldsymbol{0}) \\ \boldsymbol{S_{b3}^r} = (\boldsymbol{r_g}\ \boldsymbol{0}) \end{cases} \tag{4}$$

The above constrained screw system represents three independent constrained forces. This one can find the equivalent screw system of the mechanism

$$\boldsymbol{S_b} = \begin{cases} \boldsymbol{S_{b1}} = (\boldsymbol{r_e}\ \boldsymbol{0}) \\ \boldsymbol{S_{b2}} = (\boldsymbol{r_f}\ \boldsymbol{0}) \\ \boldsymbol{S_{b3}} = (\boldsymbol{r_g}\ \boldsymbol{0}) \end{cases} \tag{5}$$

For the parallel mechanism with the spherical six-bar kinematic chain of link mechanism, it's shown that the type 3-3RRS parallel mechanism has three rotational degrees of freedom in the $\boldsymbol{r_e}$、$\boldsymbol{r_f}$、$\boldsymbol{r_g}$ direction.

B. The kinematic of the spherical parallel mechanism

The spherical parallel mechanism's initial position is shown in Fig. 2. It can be obtained from the analysis of the figure. At this time, the two planes of the upper and lower platforms are in a parallel state, and the driving link and driven link of each branch chain are arranged in a straight line in turn.

In the $O-XYZ$ coordinate system, the coordinates of the parallel mechanism A_i、B_i and C_i are as follows:

$$R_1 = \begin{bmatrix} cos\alpha & -sin\alpha & 0 \\ sin\alpha & cos\alpha & 0 \\ 0 & 0 & 1 \end{bmatrix} \tag{6}$$

$$R_2 = \begin{bmatrix} cos\beta & 0 & sin\beta \\ 0 & 1 & 0 \\ -sin\beta & 0 & cos\beta \end{bmatrix} \tag{7}$$

$$R_3 = \begin{bmatrix} 1 & 0 & 0 \\ 0 & cos\gamma & -sin\gamma \\ 0 & sin\gamma & cos\gamma \end{bmatrix} \tag{8}$$

$$\mathrm{R} = R_1 \times R_2 \times R_3 \tag{9}$$

In the $O-XYZ$, Let the connection point C_i of each driven link and the top movable part be on a spherical surface with a diameter of 1. Let the movement angle of the driving element be θ_i, where *i* is 1, 2 and 3 respectively, C_i can be obtained by Rodriguez and the exponential product formula:

$$C_i(\theta_i) = e^{\hat{a}_i\theta_i} e^{\hat{b}_i\eta_i} c_i \tag{10}$$

where $a_i, b_i,$ and c_i are A_i's unit vector, B_i's unit vector, and C_i's unit vector, and η_i is the rotation angle of the active and passive parts.

From the structural characteristics of the single joint, it can be inferred that:

$$\left\|\overline{C_iC_j}\right\|^2 = \left(C_i - C_j\right)^T \left(C_i - C_j\right) \tag{11}$$

In (11), i and j are 1, 2 and 3 respectively.

Differentiate both sides of (11)

$$dl_{ij} = \frac{\left(C_i - C_j\right)^T}{\left\|\overline{C_iC_j}\right\|} \left(dC_i - dC_j\right) \tag{12}$$

From (12), we can obtain

$$d\eta_i = J^{-1} dl \tag{13}$$

where

$$\mathrm{J} = \begin{bmatrix} \frac{(C_2 - C_1)^T}{\|\overline{C_1C_2}\|}\dot{C_1} & \frac{(C_2 - C_1)^T}{\|\overline{C_1C_2}\|}\dot{C_2} & 0 \\ 0 & -\frac{(C_3 - C_2)^T}{\|\overline{C_3C_2}\|}\dot{C_2} & \frac{(C_3 - C_1)^T}{\|\overline{C_1C_3}\|}\dot{C_3} \\ -\frac{(C_3 - C_1)^T}{\|\overline{C_1C_3}\|}\dot{C_1} & 0 & \frac{(C_3 - C_1)^T}{\|\overline{C_1C_3}\|}\dot{C_3} \end{bmatrix} \tag{14}$$

$$\dot{C_\iota} = e^{\hat{a}_i\theta_i} e^{\hat{b}_i\eta_i} \hat{b}_i c_i \tag{15}$$

$$dl = [dl_{12} \quad dl_{23} \quad dl_{13}]^T \tag{16}$$

From (16), we can obtain

$$\eta^{k+1} = \eta^k + (J^{-1} dl)^k \tag{17}$$

Combining (17) and Rodriguez with the exponential product formula, it can be calculated by (18) in the static coordinate system.

$$\boldsymbol{O}_0 = \boldsymbol{RO} \tag{18}$$

where $\boldsymbol{O}_0$ is the coordinate value in the static coordinate system and $\boldsymbol{O}$ is the coordinate value in the movable coordinate system.

The coordinate value of the spherical parallel mechanism C_i can be obtained in the $O-xyz$ coordinate system:

$$C_0 = \begin{bmatrix} C_1 \\ C_2 \\ C_3 \end{bmatrix} = \begin{bmatrix} r_2 & 0 & 0 \\ 0 & r_2 & 0 \\ 0 & 0 & r_2 \end{bmatrix} \tag{19}$$

When the spherical parallel mechanism moves, the coordinates of the spherical parallel mechanism C_i in the static coordinate system can be obtained as

$$C_i = R \times C_0 = \begin{bmatrix} \mathrm{c}\alpha\,\mathrm{c}\beta & \mathrm{c}\alpha\,\mathrm{s}\beta\,\mathrm{s}\gamma - \mathrm{s}\alpha\mathrm{c}\gamma & \mathrm{s}\alpha\,\mathrm{s}\gamma + \mathrm{c}\alpha\,\mathrm{s}\beta\,\mathrm{c}\gamma \\ \mathrm{s}\alpha\,\mathrm{c}\beta & \mathrm{c}\alpha\,\mathrm{c}\gamma + \mathrm{s}\alpha\,\mathrm{s}\beta\,\mathrm{s}\gamma & \mathrm{s}\alpha\,\mathrm{s}\beta\mathrm{c}\gamma - \mathrm{c}\alpha\,\mathrm{s}\gamma \\ -\mathrm{s}\beta & \mathrm{c}\beta\,\mathrm{s}\gamma & \mathrm{c}\beta\,\mathrm{c}\gamma \end{bmatrix} \times r_2 \tag{20}$$

When we know the three pose change angles α, β and γ of the movable platform, because the rotating pair B_i in the middle of the driven link and the spherical pair C_i on the movable platform are connected by the same driven link, the arc angle of the plane where the driven link is located is δ2. Thus, the following formula can be obtained:

$$\frac{B_i \cdot C_i}{r_1 \times r_2} = cos\delta_2 \tag{21}$$

(12) and (13) yields, the constraint equation is

$$F_i sin\theta_i + G_i cos\theta_i = H_i \ \ (i = 1,2,3) \#(22)$$

Therefore, the drive angle of the parallel mechanism can be obtained as follows:

$$\theta_i = 2arctan \frac{F_i \pm \sqrt{{F_i}^2 + {G_i}^2 - {H_i}^2}}{H_i + G_i} \tag{23}$$

C. Positive kinematics and inverse kinematics of the continuum manipulator

It's shown the kinematic model of the continuum manipulator in Fig. 3. This paper adopts the equivalent D-H calculation formula to analyze the kinematics [27]-[28].

The transformation matrix T from the base coordinate system of the manipulator to the end can be obtained:

$${}^{j-1}_{j}T_j = \begin{bmatrix} \mathrm{c}\alpha_j\,\mathrm{c}\beta_j & \mathrm{c}\alpha_j\,\mathrm{s}\beta_j\,\mathrm{s}\gamma_j - \mathrm{s}\alpha_j\mathrm{c}\gamma_j & \mathrm{s}\alpha_j\,\mathrm{s}\gamma_j + \mathrm{c}\alpha_j\,\mathrm{s}\beta_j\,\mathrm{c}\gamma_j & 0 \\ \mathrm{s}\alpha_j\,\mathrm{c}\beta_j & \mathrm{c}\alpha_j\,\mathrm{c}\gamma_j + \mathrm{s}\alpha_j\,\mathrm{s}\beta_j\,\mathrm{s}\gamma_j & \mathrm{s}\alpha_j\,\mathrm{s}\beta_j\mathrm{c}\gamma_j - \mathrm{c}\alpha_j\,\mathrm{s}\gamma_j & 0 \\ -\mathrm{s}\beta_j & \mathrm{c}\beta_j\mathrm{s}\gamma & \mathrm{c}\beta_j\mathrm{c}\gamma_j & 0 \\ 0 & 0 & 0 & 1 \end{bmatrix} \tag{24}$$

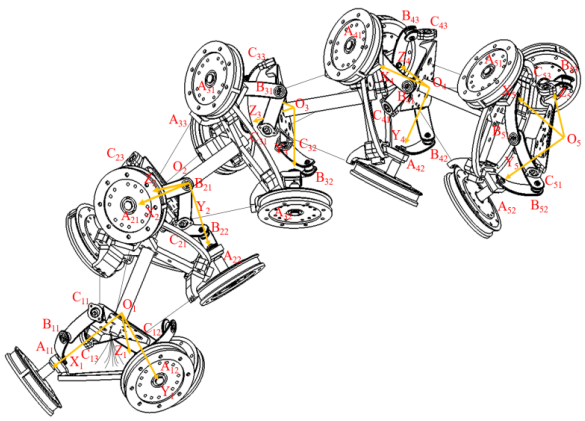

Fig. 3. The continuum manipulator

Since the continuum robotic arm is connected by multiple joints, the manipulator from static coordinates O-XYZ to dynamic coordinates $O_j - X_jY_jZ_j$, using the chain rule in the robot kinematics analysis, the homogeneous transformation matrix can be obtained:

$$ {}^{0}_{j}T_j = {}^{0}_{1}T_1{}^{1}_{2}T_2 \cdots {}^{j-1}_{j}T_j \tag{25} $$

For solving the three driving angles $\theta_{ji}(j = 1 \cdots n, i = 1 \cdots 3)$ of each continuous segment of the manipulator,the inverse kinematics analysis of the continuum manipulator is need to be known. In this paper, the driving angles of each continuous segment of the manipulator are all solved concerning the static coordinate system of each parallel mechanism. Using the same kinematic analysis method as the continuous segment, the driving angle solution formula of each parallel mechanism is obtained:

$$ \theta_{ji} = 2\arctan {}^{j-1}_{j}T_j\left(\frac{F_i \pm \sqrt{{F_i}^2 + {G_i}^2 - {H_i}^2}}{H_i + G_i}\right) \tag{26} $$

IV. Static Analysis of the Continuum Manipulator

It's shown that the continuum manipulator consists of several identical parts in Fig. 4. When the continuum manipulator is installed horizontally, the root is subjected to the greatest force. Therefore, the static analysis of the continuum manipulator is carried out using the horizontal installation structure arrangement. At this moment, the gravity itself is G_1, the gravity of the end manipulator and the grasped object is G_2, and the distances between the continuum manipulator's gravity center and gravity center of the object are L_1 and L_2, respectively, as illustrated in Fig. 4.

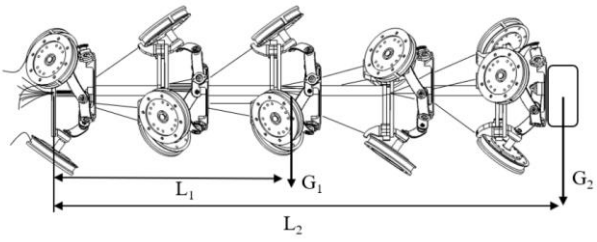

Fig. 4. The overall force of the continuum manipulator

Because each robotic arm drive unit moves independently, the drive unit close to the end of the manipulator and the drive rope close to the uppermost side of the manipulator receive the greatest force. Considering extreme conditions, only one driving rope is stressed, and it can be known from the torque balance condition that the maximum tension that a single drive rope in the robotic arm needs to bear is

$$ F_1 = \frac{G_1L_1 + G_2L_2}{r} \tag{27} $$

where r is the cam radius.

When analyzing a single drive unit, the force of a single unit is analyzed based on the overall force. When the gravity of the drive unit at the end doesn't count, the force of the movable platform is analyzed:

$$ F_2 = G_1 + G_2 \tag{28} $$

In the static analysis of this paper, the weight of the parallel mechanism and the friction between the various connected parts need to be ignored.

Since only the external load F_2 acts on the parallel mechanism, the force direction of F_2 passes through point O of the sphere center. Therefore, the static analysis of the whole parallel mechanism is shown in Fig. 5. When the mechanism as a whole is in a state of equilibrium, the static analysis is performed on each component in turn.

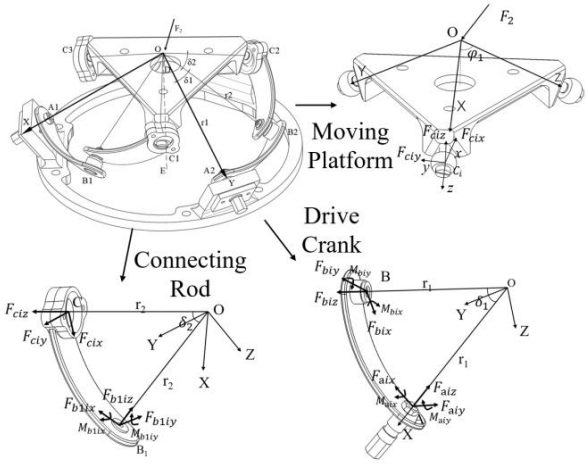

Fig. 5. Force Analysis of Parallel Mechanism

A. Static analysis of the parallel mechanism

Since the B point of the driven link and the driving link's B1 point in the linkage mechanism do not coincide at one point, the line where the driving link OB is located coincides with the line where the driving link OB1 is located. When the angle value between the driving link and the driven link is φ, according to the homogeneous transformation matrix [28]-[30], the relationship between the two coordinates can be obtained as

$$ \mathrm{R} = \begin{bmatrix} \cos\varphi & -\sin\varphi & 0 \\ \sin\varphi & \cos\varphi & 0 \\ 0 & 0 & 1 \end{bmatrix} \tag{29} $$

Therefore, the force at point B and the force at point B1 can be calculated by $\mathrm{R} \cdot F_{b1ix}$; then, under the interaction relationship of the force, we can obtain:

$$ F_{bix} = F_{b1ix}\cos\varphi \tag{30} $$

$$F_{biy} = F_{b1ix} \sin \varphi \tag{31}$$

$$F_{biz} = F_{b1iz} \tag{32}$$

Through the force analysis of the kinematic link and the movable platform. Analyze and simplify movable platforms, and a new statics formula of the movable platform is obtained:

$$F_2 + \sum_{i=1}^{3} (F_{cix} + F_{ciz}) = 0 \tag{33}$$

$$\sum_{i=1}^{3} (F_{cix} + F_{ciy}) R_1 = 0 \tag{34}$$

Simplifying F_2, F_{cix}, and F_{ciz} to O-XYZ, it can get:

$$\begin{cases} F_{c1xx} + F_{c1xy} + F_{c1z} = F_{2z} \\ F_{c2xy} + F_{c2xz} + F_{c2z} = F_{2x} \\ F_{c3xx} + F_{c3xz} + F_{c3z} = F_{2y} \\ F_{c1xy} + F_{c2xx} = 0 \\ F_{c1xz} + F_{c3xy} = 0 \\ F_{c2xy} + F_{c3xx} = 0 \end{cases} \tag{35}$$

Through the force analysis of the kinematic link and the mobile platform, get the new stress condition of the driving link:

$$\begin{cases} F_{biz} \cos \delta_1 - F_{bix} \sin \delta_1 = F_{aiz} \\ F_{biz} \sin \delta_1 - F_{bix} \cos \delta_1 = F_{aix} \\ F_{aiy} = F_{b1ix} \sin \varphi \\ M_{bix} \sin \delta_1 + F_{bix} \cdot \sqrt{2r_1^2 (1 - \cos \delta_1)} = 0 \\ F_{bix} = F_{b1ix} \cos \varphi \\ F_{biy} = F_{b1ix} \sin \varphi \end{cases} \tag{36}$$

B. Static analysis of cable drive

The static modeling of the continuum manipulator in this paper takes the principle of moment balance as the theoretical basis for the analysis.

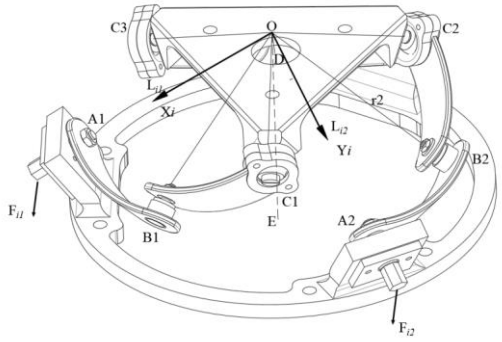

Fig. 6. The torque acting on the single parallel mechanism by the cable

As shown in Fig. 6, the i-th parallel mechanism controlled by three cables is used as a schematic for the static analysis. The respective tensions of the three driving ropes in the i-th segment are F_{i1}, F_{i2}, and. They are the column vectors relative to the static coordinate system $O_i X_i Y_i Z_i$, and the directions are shown in Fig. 6. The directions are from up to down along the pulley. Assume that the cable tension in paragraph i is as follows:

$$\begin{cases} F_{i1} = O_{r1} \cdot f_{r1} \\ F_{i2} = O_{r2} \cdot f_{r2} \\ F_{i3} = O_{r3} \cdot f_{r3} \end{cases} \tag{37}$$

where f_{r1}, f_{r2} and f_{r3} are the scalars of the ith cable tension, and O_{r1}, O_{r2} and O_{r3} are the direction vectors.

The connection lines between the contact point of the pulley and the pulley to the center point are L_{i1}, L_{i2}, and L_{i3}. The directions are from O_i to the center of the pulley, respectively. The torque generated by the cable to the center of the parallel mechanism is

$$\begin{cases} T_{i1} = L_{i1} \times F_{i1} = [Tx_{i1}, Ty_{i1}, Tz_{i1}] \\ T_{i2} = L_{i2} \times F_{i2} = [Tx_{i2}, Ty_{i2}, Tz_{i2}] \\ T_{i3} = L_{i3} \times F_{i3} = [Tx_{i3}, Ty_{i3}, Tz_{i3}] \end{cases} \tag{38}$$

where T_i is the different product of L_i and F_i, and T_i is also a column vector.

The resultant moments in the x-axis and y-axis at the parallel mechanism's center are

$$\begin{cases} Tx_i = Tx_{i1} + Tx_{i2} + Tx_{i3} \\ Ty_i = Ty_{i1} + Ty_{i2} + Ty_{i3} \end{cases} \tag{39}$$

where Tx_i and Ty_i contain three unknowns f_{r1}, f_{r2} and f_{r3}, respectively.

V. Experimental Validation

A. Construction of the experimental platform

As shown in Fig. 7, each driving pulley of the parallel mechanism is embedded with a torque sensor to measure the tensile force on the cable. Each drive cable of the parallel mechanism is led out by a pulley and fixed on the ball screw after passing through two fixed pulleys. There is an adjustment device on the ball screw to adjust the tension of the cable. The end of the ball screw contains a drive motor to drive the ball screw back and forth. The motion platform of the ball screw is fixed with a linear displacement sensor, which measures the distance traveled by the cable, thereby obtaining the rotation angle of the pulley of the parallel

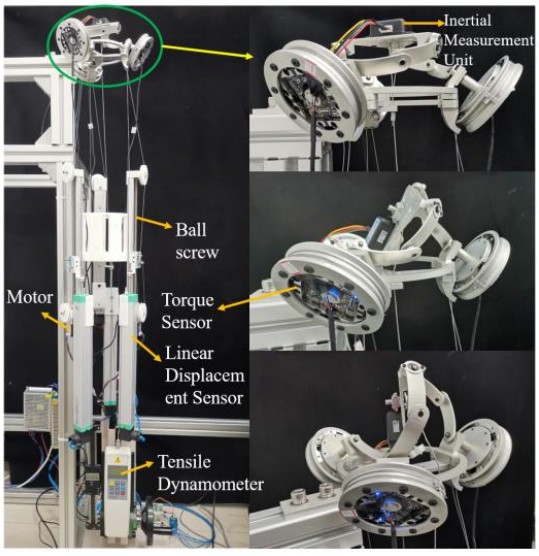

Fig. 7. The Parallel mechanism experimental platform

mechanism. A tension dynamometer is installed at the bottom of the platform of the parallel mechanism, which can apply an external load to the parallel mechanism movable platform.

B. Kinematics experiment

This experiment verifies the workspace and the motion angle of the joint's movable platform, as shown in Fig. 8 and

Fig. 9. It's shown the simulation of the kinematics theoretical model of a continuous segment in Fig. 8(a). The three coordinate systems in the figure are the rotation angles of the joint drive pulley, and the different colors represent the different rotation angles of the movable platform.

From the analysis of the movement angles in the figure, it can be concluded that the maximum movement angle of a continuous segment of the robotic arm can reach 90°. The

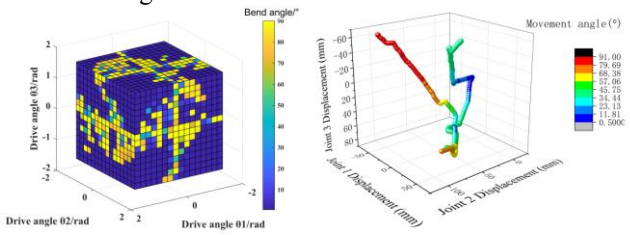

(a) Kinematic Model (b) Experimental Model

Fig. 8. The angle of motion of the continuous segments

values of the three coordinate systems in Fig. 8(b) are the length changes of the drive cables on each drive segment, and their values are measured by the linear displacement sensor. Different colors in the figure represent different rotation angles of the platform. The angles in Fig. 8(b) show that the continuous segment angle of the manipulator can reach 90°.

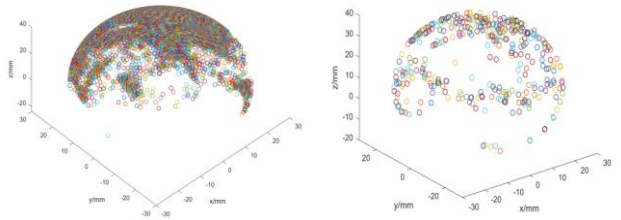

(a) Theoretical workspace (b) Experimental workspace

Fig. 9. Workspace of a continuous segment

It's shown the kinematics theory workspace of a continuous segment for the manipulator in Fig. 9(a). It's shown the workspace diagram of the continuous segment of the manipulator, which is drawn from the data measured by the inner measurement unit on the movable platform in Fig. 9(b). The experimental workspace of the parallel mechanism is a hemispherical shape.

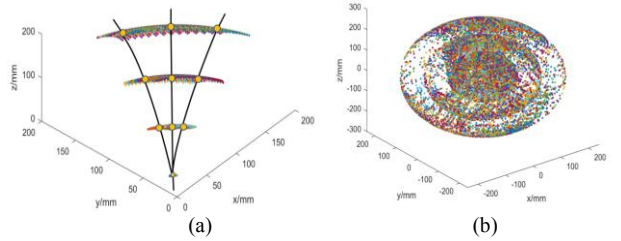

(a) (b)

Fig. 10. Workspace of the proposed continuum manipulator with four continuous segments serial connected. (a) Limit the drive angle of each segment to 30°, (b) Unrestricted driving angle of each segment

It's shown the continuum manipulator's workspace by limiting the drive angle of each continuous segment to 30° in Fig. 10(a). It's shown the workspace of the manipulator with no restriction on the drive angle of each continuous segment in Fig. 10(b). Be known from as the workspace, starting from the second joint, the workspace of each continuous segment can form a sphere except for the region of the continuum manipulator body, the robotic arm can reach any position from the second continuous segment.

C. *Statics test experiment*

This experiment verifies that different loads were applied to the movable platform, and the force of each driving pulley was measured by the torque sensor so that the driving force of each driving cable could be calculated. The force of the mechanical arm was verified.

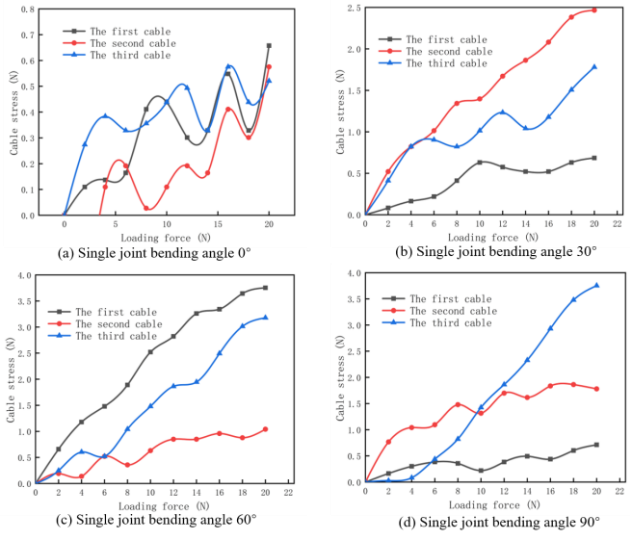

(a) Single joint bending angle 0° (b) Single joint bending angle 30°

(c) Single joint bending angle 60° (d) Single joint bending angle 90°

Fig. 11. Force analysis of a segment with different bending angles. (a) A continuous segment bending angle 0°, (b) A continuous segment bending angle 30°, (c) A continuous segment bending angle 60°, (d) A continuous segment bending angle 90°

It's shown plots the force of each drive cable of the parallel mechanism under different bending angles and load conditions in Fig. 11. With increasing load, the force of the drive cable increases to varying degrees. As the load increases, the load on the cable increases significantly. One of the three cables is also only subjected to preload. From the above analysis, it can be further proof that the continuum manipulator is under force, and there is always a drive cable under the action of the pre-tightening force.

VI. CONCLUSION

At present, most of the existing medical robots are installed with traditional rigid robotic arms, most of which have only six or less degrees of freedom, and have heavy mass and large volume. These factors make it impossible to have high flexibility in complex healthcare environments.This paper proposes a novel cable-driven spherical parallel continuum manipulator for nursing robots. The spherical parallel mechanism works as continuous segments. The kinematics and statics of the parallel mechanism of the manipulator are modeled. Finally, experiments and analysis on the single joint of the manipulator, and the kinematics and statics are verified. The results show that the platform has a large workspace and can have a large carrying capacity. We design and provide a preliminary experimental evaluation in this paper. In the next step, we will build the cable-driven system, the embedded control system, and the sensor system, as well as test the application in nursing robots.

REFERENCES

[1] D. Kolpashchikov, O. Gerget, and R. Meshcheryakov, "Robotics in Healthcare, " *Handbook of Artificial Intelligence in Healthcare*, pp. 281-306: Springer International Publishing, 2022.

[2] M. S. Sofla, M. J. Sadigh, and M. Zareinejad, "Design and dynamic modeling of a continuum and compliant manipulator with large workspace, " *Mechanism and Machine Theory,* vol. 164, 2021.

[3] D. M. Lane, J. B. C. Davies, G. Robinson, D. J. O. Brien, J. Sneddon, E. Seaton, and A. Elfstrom, "The AMADEUS dextrous subsea hand: design, modeling, and sensor processing, " *IEEE JOURNAL OF OCEANIC ENGINEERING,* vol. 24, no. 1, pp. 96-111. 1999.

[4] X. Dong, M. Raffles, S. C. Guzman, D. Axinte, and J. Kell, "Design and analysis of a family of snake arm robots connected by compliant joints, " *Mechanism and Machine Theory,* vol. 77, 2014.

[5] C. Ning, and T. Zhang, "A Portable Fully Coupled Parallel Continuum Manipulator for Nursing Robot: Mechanical Design and Modeling, " *Intelligent Robotics and Applications*, pp. 103-112: Springer International Publishing, 2022.

[6] "A Snake-Inspired Layer-Driven Continuum Robot, " *Soft Robotics,* vol. 9, no. 4, pp. 788-797. 2022.

[7] G. Qin, A. Ji, Y. Cheng, W. Zhao, H. Pan, S. Shi, and Y. Song, "A Snake-Inspired Layer-Driven Continuum Robot, " *Soft Robotics*. 2021.

[8] H. Yuan, E. Courteille, and D. Deblaise, "Static and dynamic stiffness analyses of cable-driven parallel robots with non-negligible cable mass and elasticity, " *Mechanism and Machine Theory,* vol. 85, 2015.

[9] Q. Zhang, L. Zhou, and Z. Wang, "Design and implementation of wormlike creeping mobile robot for EAST remote maintenance system, " *Fusion Engineering and Design,* vol. 118, 2017.

[10] R. Buckingham, "Snake arm robots for flexible delivery, " vol. 44, pp. 150-151, 03/01. 2002.

[11] X. Wei, Y. Zhang, F. Ju, H. Guo, B. Chen, and H. Wu, "Design and analysis of a continuum robot for transnasal skull base surgery, " *The International Journal of Medical Robotics and Computer Assisted Surgery,* vol. 17, no. 6, 2021-12-01. 2021.

[12] J. Barrientos-Diez, X. Dong, D. Axinte, and J. Kell, "Real-Time Kinematics of Continuum Robots: Modelling and Validation, " *Robotics and Computer-Integrated Manufacturing,* vol. 67, 2021.

[13] S. Bai, X. Li, and J. Angeles, "A review of spherical motion generation using either spherical parallel manipulators or spherical motors, " *Mechanism and Machine Theory,* vol. 140, 2019.

[14] P. Guardiani, D. Ludovico, A. Pistone, H. Abidi, I. Zaplana, J. Lee, D. G. Caldwell, and C. Canali, "Design and Analysis of a Fully Actuated Cable-Driven Joint for Hyper-Redundant Robots With Optimal Cable Routing, " *Journal of Mechanisms and Robotics,* vol. 14, no. 2, pp. 1-13, 2022-04-01. 2022.

[15] H. Yuan, L. Zhou, and W. Xu, "A comprehensive static model of cable-driven multi-section continuum robots considering friction effect, " *Mechanism and Machine Theory,* vol. 135, 2019.

[16] H. Yuan, W. Zhang, Y. Dai, and W. Xu, "Analytical and numerical methods for the stiffness modeling of cable-Driven serpentine manipulators, " *Mechanism and Machine Theory,* vol. 156, 2021.

[17] B. Zhao, L. Zeng, Z. Wu, and K. Xu, "A continuum manipulator for continuously variable stiffness and its stiffness control formulation, " *Mechanism and Machine Theory,* vol. 149, 2020.

[18] K. P. Ashwin, S. K. Mahapatra, and A. Ghosal, "Profile and contact force estimation of cable-driven continuum robots in presence of obstacles, " *Mechanism and Machine Theory,* 2021.

[19] T. Su, L. Niu, G. He, X. Liang, L. Zhao, and Q. Zhao, "Coordinated variable impedance control for multi-segment cable-driven continuum manipulators, " *Mechanism and Machine Theory,* vol. 153, 2020.

[20] S. Kawamura, H. Kino, and C. Won, "High-speed manipulation by using parallel wire-driven robots, " *ROBOTICA,* vol. 18, no. 1, pp. 13-21. 2000.

[21] A. Pott, H. Mütherich, W. Kraus, V. Schmidt, P. Miermeister, T. Dietz, and A. Verl, "Cable-driven parallel robots for industrial applications: The IPAnema system family. " pp. 1-6.

[22] P. Wilkening, F. Alambeigi, R. J. Murphy, R. H. Taylor, and M. Armand, "Development and Experimental Evaluation of Concurrent Control of a Robotic Arm and Continuum Manipulator for Osteolytic Lesion Treatment, " *IEEE Robotics and Automation Letters,* vol. 2, no. 3, pp. 1625-1631. 2017.

[23] M. Wang, X. Dong, W. Ba, A. Mohammad, D. Axinte, and A. Norton, "Design, modelling and validation of a novel extra slender continuum robot for in-situ inspection and repair in aeroengine, " *Robotics and Computer-Integrated Manufacturing,* vol. 67, 2021.

[24] P. Wang, S. Guo, X. Wang, and Y. Wu, "Design and Analysis of a Novel Variable Stiffness Continuum Robot With Built-in Winding-Styled Ropes, " *IEEE Robotics and Automation Letters,* vol. 7, no. 3, pp. 6375-6382. 2022.

[25] S. Bai, M. R. Hansen, and J. Angeles, "A robust forward-displacement analysis of spherical parallel robots, " *Mechanism and Machine Theory,* vol. 44, no. 12, pp. 2204-2216, 2009/12/01/. 2009.

[26] S. Bai, "Optimum design of spherical parallel manipulators for a prescribed workspace, " *Mechanism and Machine Theory,* vol. 45, 2010.

[27] A. Gao, R. J. Murphy, H. Liu, I. I. Iordachita, and M. Armand, "Mechanical Model of Dexterous Continuum Manipulators With Compliant Joints and Tendon/External Force Interactions, " *IEEE/ASME Transactions on Mechatronics,* vol. 22, no. 1, pp. 465-475, 2017-02-01. 2017.

[28] D. C. Rucker, and R. J. Webster Iii, "Statics and Dynamics of Continuum Robots With General Tendon Routing and External Loading, " *IEEE Transactions on Robotics,* vol. 27, no. 6, pp. 1033-1044, 2011-12-01. 2011.

[29] Z. Xiangzhou, L. Yougao, D. Zhiyong, and B. Hongzan, "Statics of rotational 3-UPU parallel mechanisms based on principle of virtual work. " pp. 1954-1959.

[30] S. Hasanzadeh, and F. Janabi-Sharifi, "An Efficient Static Analysis of Continuum Robots, " *Journal of Mechanisms and Robotics,* vol. 6, no. 3. 2014.